THE JOURNAL OF PHYSICAL CHEMISTRY B

Article

pubs.acs.org/JPCB

The Enolization Chemistry of a Thioester-Dependent Racemase: The 1.4 Å Crystal Structure of a Reaction Intermediate Complex Characterized by Detailed QM/MM Calculations

Satyan Sharma,[†] Prasenjit Bhaumik,[‡,∥] Werner Schmitz,[§] Rajaram Venkatesan,[†] J. Kalervo Hiltunen,[†] Ernst Conzelmann,[§] André H. Juffer,[†] and Rik K. Wierenga*[,†]

[†]Biocenter Oulu and Department of Biochemistry, University of Oulu, P.O. Box 3000, Oulu, FI-90014, Finland

[‡]Protein Structure Section, Macromolecular Crystallography Laboratory, National Cancer Institute, Frederick, Maryland 21702, United States

[§]Theodor-Boveri-Institut für Biowissenschaften (Biozentrum) der Universität Würzburg, Am Hubland, D-97074 Würzburg, Germany

Supporting Information

ABSTRACT: In the active site of the bacterial α-methylacyl-CoA racemase of *Mycobacterium tuberculosis* (MCR), the chirality of the 2-methyl branched C2-atom is interconverted between (*S*) and (*R*) isomers. Protein crystallographic data and quantum mechanics/molecular mechanics (QM/MM) computational approaches show that this interconversion is achieved via a planar enolate intermediate. The crystal structure, at 1.4 Å, visualizes the mode of binding of a reaction intermediate analogue, 2-methylacetoacetyl-CoA, in a well-defined planar enolate form. The computational studies confirm that in the conversion from (*S*) to (*R*), first a proton is abstracted by Nδ1 (His126), and subsequently the planar enolate form is reprotonated by Oδ2 (Asp156). The calculations also show that the negatively charged thioester oxygen of the enolate intermediate is stabilized by an oxyanion hole formed by N (Asp127), as well as by the side chain atoms of the catalytic residues, Asp156 and His126, both being protonated simultaneously, at the intermediate stage of the catalytic cycle. The computational analysis also reveals that the conversion of the (*S*)- to (*R*)- chirality is achieved by a movement of 1.7 Å of the chiral C2-carbon, with smaller shifts (approximately 1 Å) of the carbon atom of the 2-methyl group, the C3-atom of the fatty acid tail, and the C1-carbon and O1-oxygen atoms of the thioester moiety.

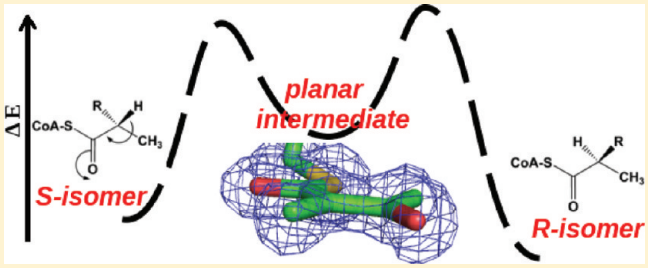

1. INTRODUCTION

The enzyme α-methylacyl-CoA racemase (AMACR; E.C. 5.1.99.4) catalyzes the interconversion of (2*R*)-methylacyl-CoA and (2*S*)-methylacyl-CoA (Scheme 1).[1,2] The racemase catalyzes this interconversion by a 1,1-proton transfer reaction using a catalytic acid/base pair.[3−5] Detailed studies of the reaction mechanism of mandelate racemase highlight the importance of the stabilization of the deprotonated intermediate[6] and of a conformational change of the side chain of the substrate.[7] AMACR is a peroxisomal as well as a mitochondrial enzyme that plays a crucial role in the metabolism of 2-methyl branched fatty acid molecules.[8] It is a dimeric protein, and for the catalytic conversion no cofactors or metal ions are required.[9] The β-oxidation enzymes that are able to metabolize 2-methyl branched fatty acyl-CoA molecules are specific for (2*S*)-chirality,[2,10,11] whereas many naturally occurring branched chain fatty acids, such as phytanic acid (3*R*/*S*,7*R*,11*R*,15-tetramethylhexadecanoic-acid), have methylations with the (*R*)-configuration. Therefore, a conversion from (*R*)- to (*S*)-configuration is required to allow shortening of fatty acids with 2-methyl branched acyl chains in β-oxidation.

The enzyme also plays a pivotal role in bile acid synthesis: during conversion of cholesterol to bile acids, oxidation of the sterol side chain specifically produces the (25*R*) diastereomer.[2,12] For shortening of the side chain by peroxisomal β-oxidation, the activated trihydroxycoprostanoyl-CoA must be converted into the (25*S*) stereoisomer.[10] Human patients with AMACR deficiency[13] as well as mouse knockout models[14] show severely disturbed patterns of bile acid compositions.

AMACR was first identified and described by Schmitz and Conzelmann.[15] Detailed studies have been reported on the enzyme from rat, mouse, and human.[10,16] Sequence alignments have revealed a number of bacterial genes with a high sequence similarity to mammalian AMACRs,[1] but so far only a few have been characterized. These are AMACRs from *Gordonia polyisoprenivorans* and *Nocardia farcinica*[17] and AMACR from *Mycobacterium tuberculosis*.[1]

Since the bacterial expression of recombinant native mammalian AMACRs results in proteins with reduced specific

Received: October 24, 2011
Revised: February 20, 2012
Published: February 23, 2012

Scheme 1. The Proposed Catalytic Cycle of AMACR

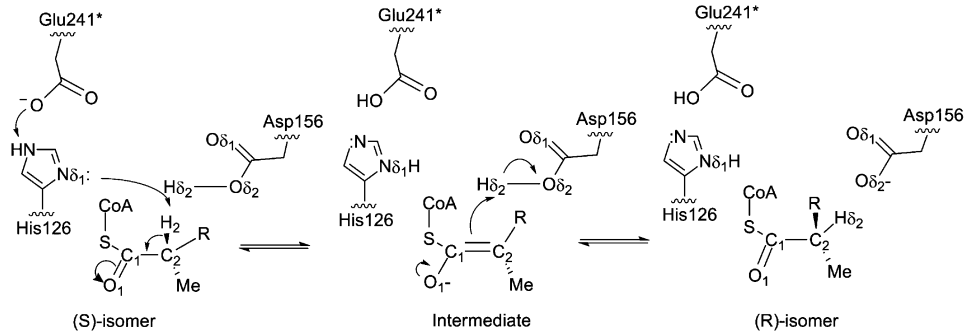

activity, the focus has been switched to an AMACR from *M. tuberculosis*, referred to as MCR. In *M. tuberculosis*, at least two homologous racemases have been identified: fatty acid-CoA racemase (FAR) and MCR. Although the crystal structure of FAR has also been reported,[18] MCR is now the best studied AMACR. Several high resolution crystal structures of MCR-substrate complexes are available.[1,9] MCR has approximately 40% sequence identity to human and rat AMACR.[1] The directly measured k_{cat} and K_M values of MCR have been reported recently,[19] showing it to be a fast enzyme. The k_{cat} and K_M are 450 sec^{-1} and 86 μM, respectively, for the conversion of the substrate (2*S*)-ibuprofenoyl-CoA into (2*R*)-ibuprofenoyl-CoA (Chart 1), whereas the k_{cat} and K_M were found to be 291 sec^{-1} and 48 μM, respectively, for the conversion of the substrate (2*R*)-ibuprofenoyl-CoA into (2*S*)-ibuprofenoyl-CoA.

Chart 1. The Covalent Structures of (A) Ibuprofenoyl-CoA (substrate) and (B) 2-meAcAc-CoA, in Equilibrium with the Deprotonated Planar 2-meAcAc-Moiety (the Reaction Intermediate Analogue), and the QM Models of (C) IBUCOA and (D) ALKCOA[a]

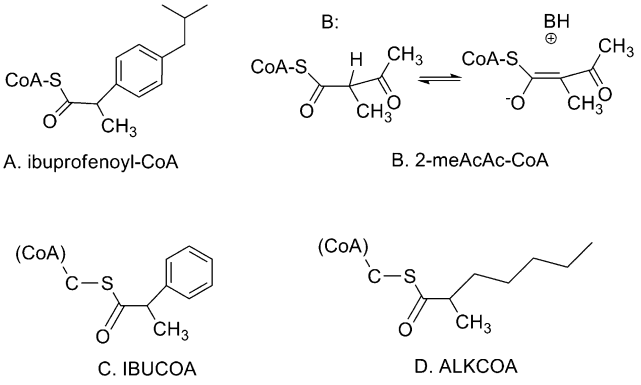

[a]The atoms of the QM models are explicitly shown.

The studies of human AMACR have become more important recently, as it has been found that human AMACR levels are a good marker for prostate cancer,[20,21] although the rationale for this is not clear.[2] These observations also have initiated research toward obtaining tight binding AMACR-inhibitors.[22] Also, enzyme mechanistic studies of human AMACR have been initiated.[23,24]

Crystal structures of MCR of the unliganded enzyme as well as the structures of various complexes have been reported.[1,9] On the basis of these structural studies, a hypothesis on the reaction mechanism has been put forward according to which the catalytic cycle is characterized by one planar enolate intermediate, which has a negative charge on the thioester oxygen (Scheme 1). The reaction of this enzyme is referred to as a 1,1-proton shift, in which a C−H proton has to be abstracted by a catalytic base from one side of the Cα-carbon of a 2-methyl branched fatty acyl-CoA molecule and donated back by a catalytic acid on the other side, or vice versa, as schematically illustrated in Scheme 1. The chemistry of this epimerase reaction is also referred to as enolizing chemistry, because the reactive carbon atom is adjacent to the carbonyl function of the thioester moiety of CoA. In order to achieve a high catalytic rate, the racemase has to lower the kinetic barrier related to proton abstraction, as well the thermodynamic barrier related to the formation of the unstable enolate intermediate.[25,26] The enolizing chemistry has also been studied for some other CoA-dependent enzymes, for example, citrate synthase,[27] crotonase,[28] and thiolase.[29] In each of these enzymes, the negative charge developing on the carbonyl oxygen atom is electrostatically stabilized by favorable interactions in an oxyanion hole.

Oxyanion holes were first described for the active sites of serine proteases, such as chymotrypsin, where they are built from two main chain NH-protons stabilizing the negatively charged tetrahedral intermediate.[30] In some related active sites, such as acetylcholine esterase, the oxyanion hole stabilizing the tetrahedral intermediate is made by three NH-groups.[31] The oxyanion holes stabilizing the enolate intermediate are much less characterized, as reviewed recently.[32] It has been noted that enolate-stabilizing oxyanion holes have a less well conserved geometry. In some cases, they are built by two main chain NH-groups (for example in the crotonase super family),[33] but in some other active sites, they are also built by two side chains, like in triosephosphate isomerase,[34] or by a side chain and a water molecule, like in thiolase and citrate synthase.[32] Studying the critical determinants of the precise geometry of these complexed active sites for the transition state stabilization in enolizing enzymes is an active area of research.[35−37]

As is shown in Figure 1, the active site of MCR is at the dimer interface. The complete dimer can be referred to as an intertwined complex of two peptide chains. The N-terminal part of each peptide chain is folded into a compact domain, followed by a protruding domain (residues 220−303), which reaches the active site of the other subunit of the dimer. Subsequently, residues 304−360 form an extensive C-terminal tail, which folds back on itself, such that the N-terminal and C-terminal ends are close together. The available crystal structures of the MCR complexes suggest that the catalytic base and catalytic acid of MCR are Asp156 and the histidine of the Glu241-His126 dyad, respectively.[9] This dyad is actually near the dimer interface, as Glu241 is provided by the other subunit

dx.doi.org/10.1021/jp210185m | J. Phys. Chem. B 2012, 116, 3619−3629

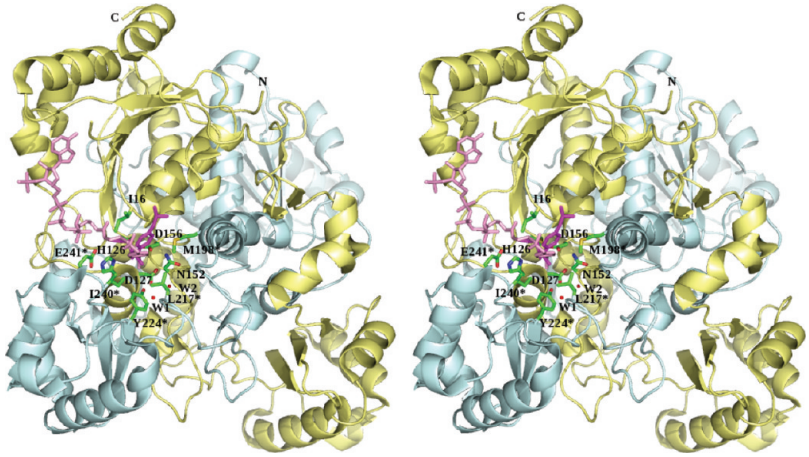

Figure 1. Overall structure of the MCR-ibuprofenoyl-CoA complex (stereo), highlighting the active site at the dimer interface (PDB entry: 2GCE). The active site occupancies of the *R* and *S* substrate molecules are 0.5, respectively. Also shown are the side chains of Ile16, His126, Asp127, Asn152, Asp156, Met188, Met198*, Leu217*, Tyr224*, Ile240*, and Glu241*. The N and C termini of the reference subunit and the side chains of the important residues are labeled. Also shown are the two conserved active site waters (W1 and W2).

of the dimer. This Glu241 will therefore be referred to as Glu241*. The side chain of Asp156 is anchored between Sδ (Met188) and Nδ1 (Asn152) (Figure 1). His126 is the base when the substrate is (2*S*)-ibuprofenoyl-CoA (Asp156 is the acid in this direction), whereas Asp156 is the base when (2*R*)-ibuprofenoyl-CoA is the substrate. The thioester oxygen of the substrate is hydrogen bonded to the main chain N (Asp127).

Many structural studies have been aimed at capturing the structure of serine proteases complexed with its tetrahedral intermediate. This has been achieved by trapping intermediate structures in two ways: either by using pH jump approaches,[38] or by using suitable substrate soaking conditions.[39] For enolizing enzymes, however, only structures of complexes with substrate or substrate-like molecules are available.[32] To elucidate the binding of a planar reaction intermediate and the precise geometry of the complexed oxyanion hole, we report on the 1.4 Å resolution crystal structure of MCR with a bound reaction intermediate analogue. Further, computational approaches were employed to gain an understanding of the reaction mechanism of MCR. These calculations provide interesting and new insight into the reaction mechanism and in the oxyanion hole properties of this enzyme, showing that the catalytic acids (His126, Asp156) of the active site have a dual role, being a proton donor/acceptor in the 1,1-proton shift mechanism as well as being part of the oxyanion hole, stabilizing the enolate reaction intermediate.

2. EXPERIMENTAL PROCEDURE

2.1. Crystallization and Ligand Soaking. MCR was purified and crystallized as described previously.[9] Briefly, the crystals were grown by the vapor diffusion method using hanging drops made by mixing 3 μL of reservoir solution (1.52 M ammonium phosphate, 10 mM $BaCl_2$ at pH 7.0) with 3 μL protein solution (6 mg/mL in 10 mM potassium phosphate buffer, pH 8.8). The crystals were grown at room temperature and harvested after 14 days. Subsequently, the crystals were transferred to a drop of mother liquor, also containing 2 mM 2-methylacetoacetyl-CoA (2-meAcAc-CoA). 2-meAcAc-CoA was synthesized from a racemic mixture of the ethylester of 2-methylacetoacetate, as described previously.[40] The K_d of the complex of MCR and 2-meAcAc-CoA was found to be 120 μM, using a competitive inhibition assay, as described previously.[9] After a 4 h soak, the crystals were transferred to a cryosolution (mother liquor, also containing 15% glycerol, as well as 2 mM 2-meAcAc-CoA) for 15 s and frozen in a cold nitrogen gas stream.

2.2. Data Collection and Structure Refinement. The frozen crystal was stored in liquid nitrogen and transferred to the ESRF synchrotron in Grenoble (France). The 1.4 Å data set was collected on beamline ID14-2, equipped with an ADSC Quantum 4 CCD-detector. The data set was processed using the program package XDS.[41,42] Further data manipulations were done with programs of the CCP4 package.[43] The structure of the complex was determined by molecular replacement using the program MOLREP.[44] The CD dimer of the ibuprofenoyl-CoA-MCR complex (PDB access code: 2GCE) was used as the search model, after removing the ligands in the active sites. The structures were refined via iterative cycles of model refinement with REFMAC5[45] and model building in electron density maps using Coot.[46] The data collection statistics and refinement statistics are listed in Table 1. The coordinates of the refined structure have been submitted to the PDB (ID code: 2YIM).

2.3. Structure Analysis. The asymmetric unit contains two MCR dimers. The 2-meAcAc-CoA molecule is very well-defined in each of the four subunits. The four catalytic centers are identical. In the structure description, subunit A is used as the reference active site; residues of the B subunit complement this active site. The comparisons are also performed with the crystal structures of the complex with ibuprofenoyl-CoA (2GCE), (2*S*)-methylmyristoyl-CoA (2GD0), (2*R*)-methylmyristoyl-CoA (2GCI), and acetoacetyl-CoA (2GD2), as well as the unliganded structure (1X74). The images of Figures 1−4, 7, and 9 have been made with PyMOL.[47]

2.4. Set-up of the Computational System. The models for the computational studies are based on the crystal structure of MCR complexed with ibuprofenoyl-CoA (2GCE) and (2*S*)-methylmyristoyl-CoA (2GD0) (Chart 1), respectively. The D active site of the CD-dimer has been used in the calculations. The missing residues, residues 40−44, were modeled using Modeler.[48] This surface loop is far away from the catalytic site, and this modeling has not changed the rest of the structure. The protonation states of the residues directly involved in catalysis were assigned according to the proposed reaction

Table 1. Crystallographic Data

Data Collection Statistics	
beamline	ID14-2
wavelength (Å)	0.933
temperature (K)	100
space group	*C*2
V_M (Å^3/Da)	2.7
No. of subunits/a.s.u	4
Unit Cell Parameters	
a, *b*, *c* (Å)	181.6, 80.2, 118.9
β (°)	91.4
resolution range (Å)[a]	21.37−1.41(1.49−1.41)
R_{merge} (%)[a]	6.1(48.2)
R_{meas} (%)[a]	7.2 (57.0)
$\langle I/\sigma(I)\rangle$[a]	11.9(2.4)
completeness (%)[a]	98.7(96.9)
multiplicity[a]	3.6(3.5)
no. of unique reflections	322760
Wilson B factor (Å^2)	12.2
processing software	MOSFILM
Refinement Statistics	
resolution (Å)	21.37−1.41
R_{factor} (%)	18.6
R_{free}(%)	20.5
number of protein atoms	11410
number of ligand atoms	220
number of other solute atoms	40
number of water molecules	1825
Geometry Statistics	
rmsd bond length (Å)	0.0065
rmsd bond angles (°)	1.1
rms chiral volume (Å^3)	0.073
average B factor (Å^2)	
protein main chain	12.8
protein side chain	13.4
ligand	14.6
other solute molecules	35.0
water molecules	27.5
Ramachandran Plot (%)[b]	
favored	96.9(0.3% outliers)
allowed	2.8
outliers	0.3
PDB ID	2YIM

[a]The numbers in parentheses refer to the outer shell. [b]Done with PROCHECK.

scheme for the (*S*) to (*R*) conversion. His126 is neutral, being protonated at Nε2, but not at Nδ1. Glu241*, hydrogen bonded to Nε2 (His126), is deprotonated. Asp156 is neutral. The remaining residues were set to their normal protonation state at neutral pH. The complex was placed in a periodic dodecahedron box of dimension 790 nm^3. The crystallographic waters associated with the dimer were retained. The box was then filled with approximately 22 600 water molecules. The water molecule was described with the simple point charge (SPC) model.[49] The system was neutralized by adding counterions. A weak temperature and pressure coupling was established using the Berendsen algorithm.[50] The fast particle mesh Ewald summation technique was employed to correctly compute long-range Coulomb forces.[51] The LINCS algorithm was employed to constrain bonds.[52] The individual dimer, with bound ligand, was relaxed using 2500 steps of steepest descent followed by conjugate gradient minimization. A 300 ps restrained molecular dynamics (MD) run was then carried out by slowly increasing the temperature from 0 to 300 K during the first 30 ps, followed by equilibration at constant temperature of 300 K. During this equilibration, only the backbone atoms were restrained, while the side chain and the ligands were unrestrained. Subsequently, the system was relaxed by another round of conjugate gradient minimization. All MD simulations were performed with the GROMACS package[53,54] with the AMBER force field of ffamber99.[55]

2.5. Ligand Topologies. The topology for the 3′,5′-adenosine triphosphate moiety of the ligand was adapted from NADP$^+$.[56] The restrained electrostatic potential (RESP) charges for the pantothenic acid and the tail fragments were generated on the basis of HF/6-31G(d) quantum calculations using the ANTECHAMBER module of the AMBER program.[57] The remaining bonded parameters were taken from the literature.[58] For the ibuprofen related model (IBUCOA), the alkyl chain of the phenyl ring of ibuprofen was removed, and for the model based on the (2*S*)-myristoyl-CoA complex (ALKCOA), the alkyl chain was truncated to seven carbons (Chart 1).

2.6. Potential Energy Surface (PES) Calculations. All the quantum mechanics/molecular mechanics (QM/MM) calculations were done using the ONIOM methodology[59] with mechanical embedding, as implemented in Gaussian09.[60] For the initial generation of the Michaelis complex and the validation of the reaction coordinate, a model was constructed from the energy-minimized and MD-relaxed structure of the complex. In this system, the enzyme was modeled using all the residues within a sphere of 15 Å radius of the thioester carbonyl carbon of the substrate moiety. The N-terminal of each peptide fragment was treated as an amine, while the C-terminal was treated as an aldehyde. The structural waters within the sphere were also included in the model. The model was then divided into two layers. The inner layer consisted of a part of the ligand, complete residue His126, and side chains of Asp156, Asn152, and Glu241*. Asp156 is neutral, with the proton at the *syn*-orbital of Oδ2. In addition, the His126−Asp127 peptide bond and the Cα atom of Asp127 were also included in the inner layer. The inner layer of 75 atoms (heavy atoms plus hydrogen atoms) was treated at the HF/3-21G level. The rest of the system, comprising 4498 atoms, including 287 water molecules, was assigned to the outer layer. The outer layer was treated using the parm99 force-field parameter.[61]

A relaxed two-dimensional (2D)-PES calculation along the two plausible reaction coordinates was carried out in steps of 0.1 Å, using the complete ONIOM model. The first reaction coordinate (*r*1), is the distance between Nδ1 (His126) and the C2-proton. The second reaction coordinate (*r*2), is the distance between the Oδ2 (Asp156) hydrogen atom and the C2 of the substrate. The *r*1 was varied from 2.2 Å to 1.0 Å, considering the (*S*) to (*R*) conversion. The reaction coordinate *r*2 was varied from 3.5 Å to 2.0 Å. The position of the protein atoms beyond 12 Å of the thioester carbonyl carbon were kept frozen in these calculations. The energy contour was plotted using the MATLAB software.[62]

2.7. Transition State Calculations. For transition state (TS) calculations, smaller ONIOM models were constructed on the basis of the optimized larger ONIOM models of the reactant, intermediate, and product states. All of the inner QM region atoms (75 atoms) were included along with

Ile16−Pro18, Ala124−Tyr130, Leu151−Phe157, Met188, Met198*, Leu217*, Tyr224*, Ile240*−Glu241*, and Phe244* residues (the asterisks indicate residues from the other subunit of the dimer) and nearby waters in the MM region (total 458 atoms). As in the larger ONIOM model, the N-termini of the peptide fragments were treated as an amine, while the C-termini were treated as an aldehyde. The inner layer was treated at HF/6-31G(d). The synchronous transit-guided quasi-Newton methodology (STQN) was used to locate and optimize the transition states using Gaussian09.[60] All the stationary points were characterized as either minima (all real frequencies) or transition states (only one imaginary frequency) by normal-mode analysis. Finally, the single-point energies were calculated at MP2/6-31+G(d):Amber. Atomic charges of the QM-models were obtained using the charge from an ESP grid-based (CHELPG) fitting procedure[63] as implemented in Gaussian09.

Finally, the geometry of the product, as obtained from the ONIOM calculations, was further studied. First the product geometry was relaxed in the protein environment. For this, the atomic positions from the product geometry were substituted in the previously MD relaxed protein structure. After this, the position of the atoms corresponding to the ONIOM model were restrained and the system was energy minimized. This was then followed by a 300 ps position restrained MD simulation. The restraints were applied only to the heavy atoms of the protein.

3. RESULTS AND DISCUSSION

3.1. Structural Details of the MCR-2-meAcAc-CoA Complex. The crystals of the MCR-2-meAcAc-CoA complex diffract to high resolution, and the mode of binding of the 2-meAcAc-CoA is well-defined in each of the four subunits (Figure 2). In the previous crystallographic binding studies of MCR with ibuprofenoyl-CoA and 2-methylmyristoyl-CoA, the crystals suffered upon ligand binding, and these experiments could only be completed after cross-linking the crystals with glutaraldehyde.[9] This crystal deterioration could be explained because the binding site for the bulky fatty acid tail is close to a crystal contact. By contrast, the acetoacetyl moiety of 2-meAcAc-CoA is much shorter as compared to the fatty acid tails of ibuprofenoyl-CoA as well as 2-methylmyristoyl-CoA, and no crystal cracking was observed in these binding studies. The shape of the electron density of the omit (F_o−F_c) map clearly defines the mode of binding of the 2-methyl group, being bound in a pocket shaped by the side chains of residues His126 (Cβ at 3.9 Å), Asp127 (Cβ at 4.2 Å), Asn152 (Cβ at 4.1 Å), Asp156 (Oδ2 at 3.6 Å), Leu217* (Cδ2 at 3.9 Å), Tyr224* (Cζ at 4.2 Å), and Ile240* (Cδ1 at 4.2 Å) (Figure 3). Interestingly, the shape of the electron density for the ligand also clearly shows that 2-meAcAc-CoA is trapped as a planar molecule, being most likely the planar negatively charged enolate reaction intermediate (Chart 1B). Its conformation and mode of binding is the same as that observed for the acetoacetyl-moiety in the crystal structure of the MCR acetoacetyl-CoA complex (pdb code: 2GD2).[9] The thioester oxygen, O1, is closest to Asp156 (Oδ1 at 2.7 Å, Oδ2 at 3.0 Å), Asp127 (N at 2.9 Å), and His 126 (Nδ1 at 3.6 Å).

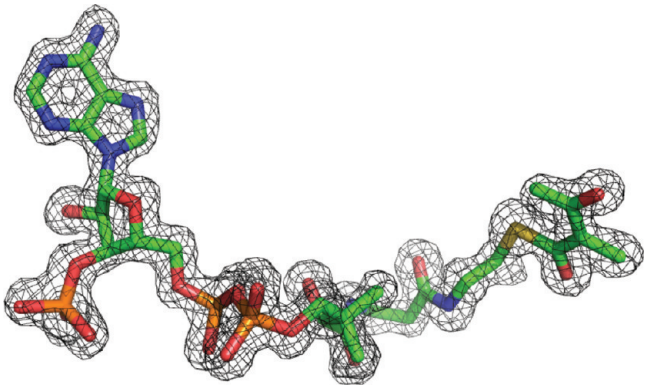

Figure 2. The omit (F_o−F_c) map calculated after omit refinement of the bound 2-meAcAc-CoA, contoured at 3.0 sigma. For the omit calculation, the shown ligand atoms have been omitted from the refinement and map calculations.

The 2-meAcAc moiety and the ibuprofen moiety have a different polarity, due to the 3-ketogroup of the 2-meAcAc group (Chart 1). Consequently, the α-proton of the 2-meAcAc moiety has a much lower pK_a, for example, the proton of the corresponding carbon of ethylacetoacetate easily exchanges with deuterium in D_2O.[64] Also, the pK_a of the α-proton of acetoacetyl-CoA is near 9,[65] whereas the pK_a of the Cα-proton of acyl-CoA is near 21.[66] The lower pK_a of the α-proton of acetoacetyl-CoA, and, by analogy, the lower pK_a of the α-proton of 2-meAcAc-CoA, makes this molecule a better reaction intermediate analogue, rather than a substrate analogue. This allowed the trapping of the negatively charged planar enolate intermediate in this crystallographic experiment.

The protein atoms closest to the chiral atom C2 of 2-meAcAc-CoA are Nδ1 (His126) at 3.5 Å and Oδ2 (Asp156) at 3.3 Å. The distance to Oδ1 (Asp156) is 4.4 Å. The comparison of the structures of the active sites of the unliganded form and the 2-meAcAc-CoA complex shows only minor differences in the active site geometry. The protein−protein hydrogen bonding interactions in the active site of the unliganded and 2-meAcAc-CoA complex, as listed in Table 2, are very similar, confirming the rigidity of the active site. The most pronounced difference is observed for the side chain of Ile16, which is rotated to allow for the binding of the sulfur of 2-meAcAc-CoA. This was also observed in the structure of the ibuprofenoyl-CoA complex. Other structural changes concern the replacement of the glycerol molecule and the water structure. In the unliganded active site, the catalytic residues His126 and Asp156 are hydrated by well-defined waters and by glycerol. In the 2-meAcAc-CoA complex, these catalytic residues are not hydrated, but are buried and closely interacting with the thioester moiety of 2-meAcAc-CoA. The side chain conformations of His126 and Asp156 are the same in the unliganded structure, the 2-meAcAc-CoA structure, and the ibuprofenoyl-CoA structure.

3.2. 1,1-Proton Transfer Mechanism and the Planar Intermediate. In order to assess the importance of the planar enolate intermediate and the geometry of the oxyanion hole for catalysis, the catalytic cycle was modeled by a QM/MM-calculation. In the modeling calculations, first the abstraction of the C2-proton of (2*S*)-IBUCOA by Nδ1 (His126) was studied, followed by the donation of the C2-proton by Oδ2 (Asp156). The initial QM/MM calculations were done using the larger ONIOM model. The QM layer was treated at the HF/3-21G level. Figure 4 shows only the active site residues of the QM-optimized reactant complex of MCR, with bound (2*S*)-IBUCOA, competent for the conversion of the (*S*) into (*R*) substrate. Also shown are the protonation states of active site

dx.doi.org/10.1021/jp210185m | J. Phys. Chem. B 2012, 116, 3619−3629

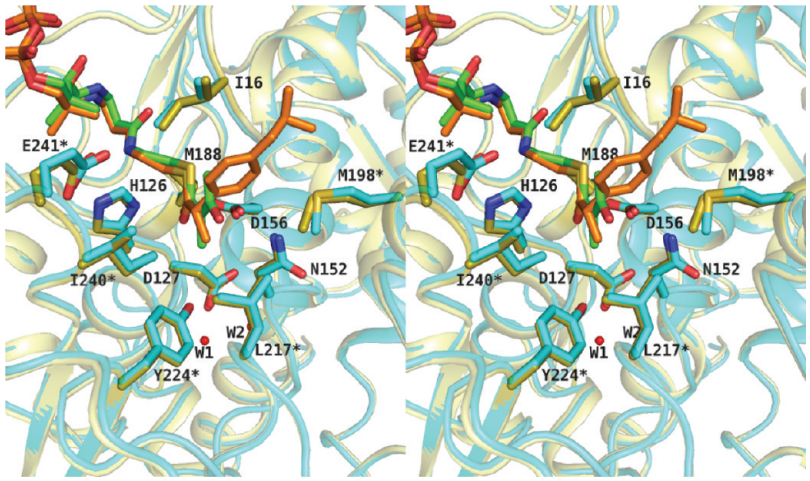

Figure 3. Comparison of the active sites of the 2-meAcAc-CoA complex (cyan) and the MCR-(2*S*)- ibuprofenoyl-CoA complex (yellow) with the ligands (2*S*)-ibuprofenoyl-CoA (orange) and 2-meAcAc-CoA (green).

Table 2. The Hydrogen Bond Distances (Å) among the Residues of the Active Site

acceptor atom	donor atom	1X74[a]	2YIM[b]	reac[c]	TS1[c]	INT[c]	TS2[c]	prod[c]
Oε1(Glu241*)	Nε2(His126)	2.6	2.7	2.8	2.7	2.8	2.7	2.7
Oδ2(Asp156)	Nδ2(Asn152)	2.9	2.9	3.2	3.4	3.2	3.0	3.0
OH(Tyr224*)	N(Ile128)	3.1	3.1	3.2	3.2	3.2	3.2	3.1
Wat2319	OH(Tyr224*)	2.5	2.7	2.7	2.7	2.7	2.7	4.5
Oδ1(Asp127)	Wat2319	2.7	2.7	2.6	2.6	2.6	2.6	2.6
Oδ2(Asp127)	N(Val154)	4.0	3.9	4.2	3.9	4.2	4.1	4.1
Oδ2(Asp127)	N(Gly155)	2.8	2.8	2.9	3.0	2.9	3.0	3.1
Oδ2(Asp127)	N(Asp156)	2.8	2.8	2.8	2.8	2.8	2.8	2.9
O(His126)	N(Asn129)	2.8	2.8	2.9	2.9	2.9	2.8	2.8
O(His126)	N(Tyr130)	3.4	3.4	3.5	3.6	3.6	3.5	3.5

[a]MCR apoenzyme. [b]MCR complex with 2-meAcAc-CoA. [c]The geometries have been taken from the 2D-PES calculations (see Figure 5).

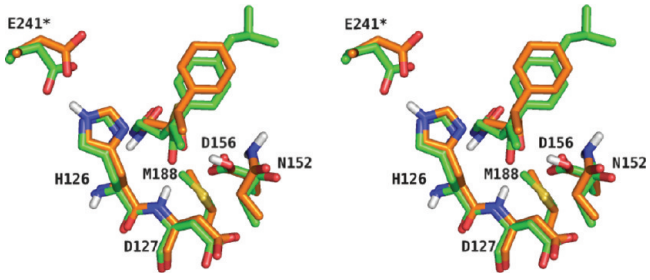

Figure 4. The active site structure of the (*S*)-ibuprofenoyl-CoA complex superimposed with ONIOM optimized reactant (IBUCOA). The X-ray structure is in green. The Asp156 acidic proton of the optimized active site (orange) is located on the *syn*-orbital of Oδ2 (Asp156). The residues of the inner QM region are His126, Asn152, Asp156, and Glu241*. Also shown are the side chains of Asp127 and Met188.

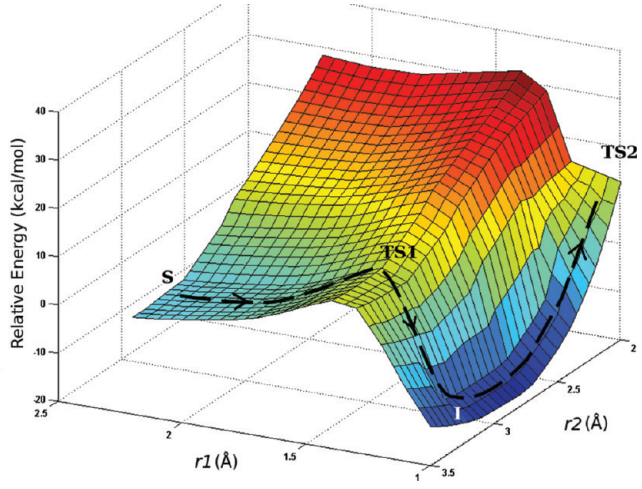

Figure 5. The 2D-energy profile of the catalytic cycle calculated at the HF/3-21G level: there is one planar intermediate. The reaction coordinate "*r*1" refers to the distance between the Nδ1 atom of His126 and the C2-hydrogen atom (H2) of IBUCOA, and "*r*2" refers to the distance between the C2 atom of IBUCOA and the Hδ2 atom of Asp156. The dashed arrow indicates the lowest energy path from the *S*-isomer reactant (S) to the second TS (TS2) passing through the first TS (TS1) and a planar intermediate (I).

residues, with the proton initially bound to Oδ2 (Asp156) and not at Nδ1 (His126).

To investigate whether or not the two proton transfer steps are sequential, a 2D-PES calculation was carried out on the fully geometric optimized model. The (*S*) to (*R*) racemization reaction was investigated in this calculation. The decreasing *r*1 results in the protonation of His126 (Figure 5). Accordingly, the decreasing *r*2 distance describes the formation of the *R* isomer of the substrate. Only a section of the 2D surface was constructed, as it clearly identified the region where the intermediate is located. The constructed PES clearly indicates that the two proton transfers are sequential, as can be deduced from the lowest energy path. The lowest energy path of the 2D-PES plot (Figure 5) is marked with arrows. Along the lowest

dx.doi.org/10.1021/jp210185m | *J. Phys. Chem. B* 2012, 116, 3619–3629

energy path (shown as a dashed arrow), several single point energy calculations at a higher level (MP2/6-31+G(d)//HF/3-21G) were also performed. At the higher level, the relative energetics of the stationary points *S*-isomer reactant (S), first transition state (TS1), planar intermediate (I), and second transition state (TS2) are 0.0, 11.7, 3.8, and 6.4 kcal/mol, respectively. The *R*-isomer product (not shown) with $r1$ = 1.0 Å and $r2$ = 1.1 Å lies at −7.1 kcal/mol relative to the *S*-isomer. Along this low energy path, the reaction passes through two transition states separated by a well-defined minimum. This minimum corresponds to a planar intermediate as the dihedral angle of O1−C1−C2−(2-methyl carbon) assumed a value of 0°, compared to 13° at the reactant state, as also observed in the studies of mandelate racemase.[26] The first TS (TS1) corresponds to the transfer of the C2-proton from the substrate to the Nδ1 of His126. With the decreasing value of $r1$ on the energy surface, a simultaneous proton transfer occurs from the (Nε2) His126 to (Oε1) Glu241*. Thus, both the His126 and Glu241* become neutral at the planar intermediate. During this first step, the Asp156 remains protonated. The second step is then the transfer of the proton from the Oδ2 atom of the neutral Asp156 to the intermediate to generate the (*R*)-isomer. Table 2 compares the hydrogen bonds in the active site of the QM/MM-models and the experimental structures, highlighting the rigidity of the active site structure during the catalytic cycle.

The two transition states were characterized by further calculations using a smaller model (see the Experimental Procedure section) and a higher basis set (HF/6-31G(d)). The TS for the abstraction of the C2-proton from the substrate by His126 was located using the STQN method in Gaussian09.[60] The energy of TS1 appears closer to the enolate intermediate than to the reactant, in accordance with Hammond's postulate, considering the energetics at MP2/6-31+G(d) (see also Figure 8). During this transfer, at first the two heavy atoms Nδ1 and C2 involved in the transfer approach closer. This is consistent with the 2D energy scan, corresponding to the initial region of minimal energy change before the reaction approaches TS1. The Nδ1−C2 distance reduces from 3.3 Å to 2.8 Å in the TS1 and again increases to 3.7 Å in the enolate intermediate. This is also very similar to the proton abstraction reaction previously observed in the mechanism of citrate synthase.[67,68] The positive charge on the proton increases from 0.04 to 0.26 units. The change in charge of the C2 atom from reactant to enolate is −0.45 units (see Figure 6). The negative charge on O1 and C1 also changes from −0.49 and 0.47 units in reactant to −0.58 and 0.32 units in the enolate intermediate, indicative of the charge delocalization. Accordingly, the length of the C1−C2 bond decreases, whereas there is a lengthening of the C1−O1 bond. The changes are qualitatively similar to the enolate intermediate previously observed in the case of citrate synthase.[68] The charge on the S atom of the CoA moiety also changes by −0.12 units in the enolate. Thus, the sulfur is also important for charge stabilization in the enolate intermediate. In the conversion of reactant to product, the largest atomic movement is seen for the C2 chiral atom (1.7 Å), smaller movements are seen for the C1 (0.8 Å), the O1 (1.0 Å), the 2-methyl carbon (1.1 Å), and the C3 atom (1.2 Å). The O1 atom moves from Oδ1/Oδ2 (Asp156) to Nδ1 (His126) (Figure 7), while the hydrogen bond to N (Asp127) is preserved (see Table 3).

The complete energy profile for the conversion of the (2*S*)-isomer to the (2*R*)-isomer is shown in Figure 8. The energy

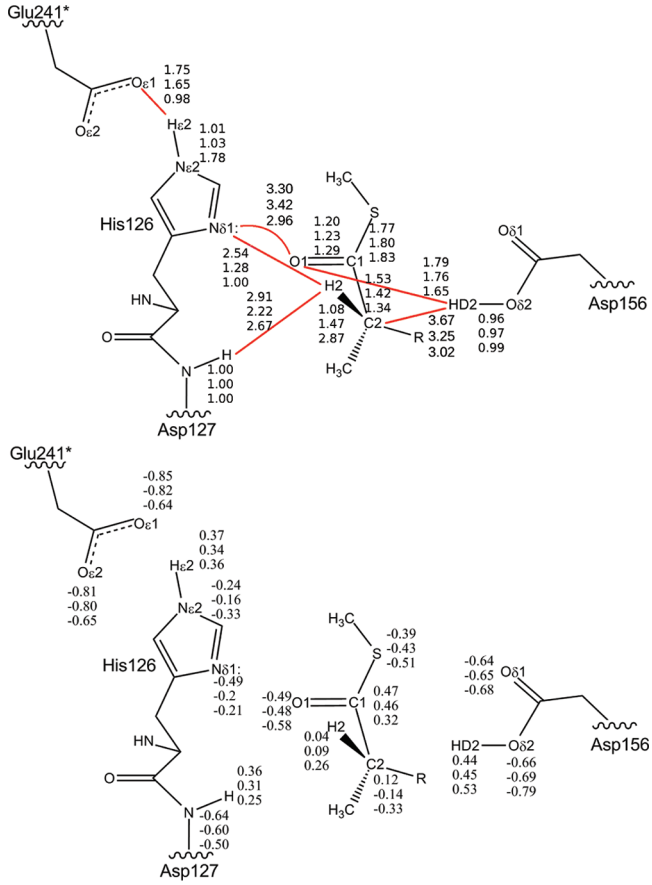

Figure 6. The interatomic distances (top panel) and calculated CHELPG (HF/6-31G(d)) atomic charges (bottom panel) for the reactants (upper values), TS1 (middle values), and the planar intermediate (lower values) for the IBUCOA complex, optimized at the HF/6-31G(d):AMBER level.

barriers for the two proton transfer steps, relative to the reactant, are very similar. The overall calculated energy barrier for conversion of (2*S*)-IBUCOA into (2*R*)-IBUCOA is 12.3 kcal/mol. This is in reasonable agreement with the experimental result of ∼13.8 kcal/mol, as calculated from the measured conversion rates (k_{cat}).[19] The *R*-isomer is seen to be ∼6 kcal/mol lower in energy with respect to the reactant, indicating a higher barrier for the conversion of the (*R*)-isomer to (*S*)-isomer, as compared to the (*S*)- to (*R*)-conversion. Experimentally, the barrier for conversion of (*R*)- to (*S*)-ibuprofenoyl-CoA is also found to be slightly higher (∼14.1 kcal/mol).[19]

The product was further relaxed in the complete protein environment using a short MD equilibration procedure. In this short relaxation step, it was observed that the aromatic ring moiety of the ligand immediately moves in response to the protein environment, to the so- called *R*-pocket, as defined in the crystal structure of the MCR-ibuprofenoyl-CoA complex (Figure 7). There are no appreciable changes in the protein structure and the CoA part of the ligand. The results support the previous observation[9] that indeed the ligand tail of the (*R*)- and (*S*)-isomers occupy different regions of the enzyme, whereas the 2-methyl group remains bound in the same pocket.

Subsequently, the calculations were repeated for the (*S*)-ALKCOA model. The stationary states showed similar geometries and essentially similar features of enolate stabilization.

dx.doi.org/10.1021/jp210185m | *J. Phys. Chem. B* 2012, 116, 3619−3629

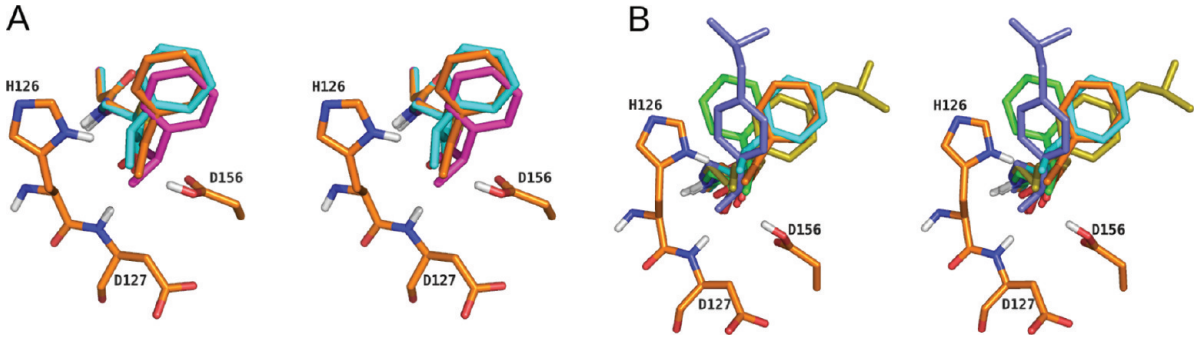

Figure 7. (A) Zoomed in stereo view of the ONIOM structures of reactant (cyan), planar intermediate (orange) and product state (magenta), visualizing the large shift of the chiral C2-atom. (B) The stereo view of superposition of X-ray structures of (*R*)-isomer (blue) and (*S*)-isomer (yellow) of ibuprofenoyl-CoA comparing the ONIOM structures of the reactant (cyan), intermediate (orange), and the QM-MD relaxed product (green).

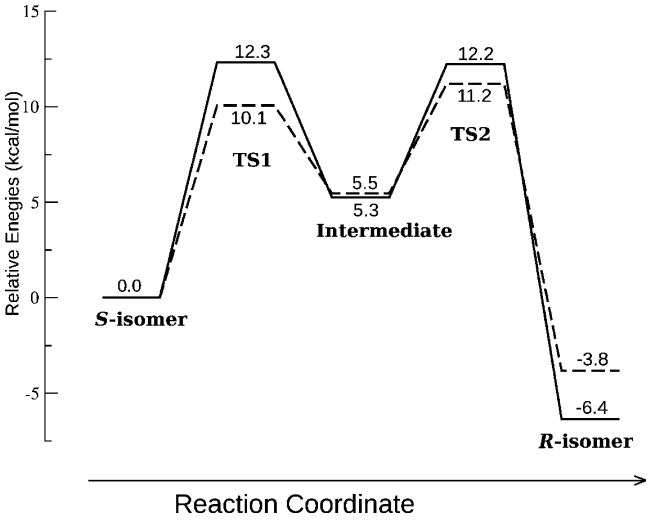

Figure 8. The energy profile of the complete catalytic cycle of the (*S*) to (*R*) conversion of IBUCOA (solid) and ALKCOA (dashed) calculated at a higher level (MP2/6-31+G(d)//HF/6-31G-(d):AMBER) using the smaller ONIOM models.

The overall energy profile is shown in Figure 8. In the case of ALKCOA, the overall barrier is slightly lower as compared to IBUCOA. The relative energy of the *R*-isomer of ALKCOA is ∼4 kcal/mol lower than the reactant energy, whereas for IBUCOA it was found to be 6.4 kcal/mol lower. This indicates that the rates of (*S*)- to (*R*)- and (*R*)- to (*S*)- conversion in the active site would be more similar to each other in the case of ALKCOA as compared to IBUCOA, the non-natural substrate homologue.

QM/MM calculations were also done for the substrate (2*S*)-meAcAc-CoA. In these calculations, it was found that the relative energy of the generated enolate intermediate is considerably lower than calculated for the IBUCOA and ALKCOA intermediate complexes. The energy of the intermediate in this case is 5.5 kcal/mol lower with respect to the reactant, whereas it is much higher for IBUCOA (5.3 kcal/mol) and ALKCOA (5.5 kcal/mol) (see Figure 8). This is in excellent agreement with the results of the crystallographic binding study with 2-meAcAc-CoA, which shows that, under the chosen experimental conditions, the planar intermediate of the 2-meAcAc-CoA substrate has been trapped in the crystallized MCR active site.

3.3. Rigidity of the Active Site and the Oxyanion Hole.

The calculations show that the catalysis proceeds with minimal conformational changes in the active site. The largest structural change is the movement of the fatty acid tail from the *S*-pocket to the *R*-pocket, which is a structural adjustment once the chemistry of the (*S*)- to (*R*)- conversion has been completed. It is interesting that the histidine side chain remains neutral in the catalytic cycle, because concomitantly with the proton transfer from the C2 atom to Nδ1 (His126), a proton is transferred from Nε2 (His126) to Oε2 (Glu241*). At this stage of the reaction, the racemization of the substrate is completed,

Table 3. The Contact Distances between the Thioester O1 and the HBDs in the Oxyanion Hole in Different Structures

	HBDs			
structures	N(Asp127)	Nδ1(His126)	Oδ1(Asp156)	Oδ2(Asp156)
acetoacetyl-CoA[a]	2.9	3.7	2.5	3.0
(2*R*)-ibuprofenoyl-CoA[b]	2.9	3.3	2.9	3.3
(2*S*)-ibuprofenoyl-CoA[b]	3.0	3.3	3.1	2.9
(2*R*)-methylmyristoyl-CoA[c]	2.6	3.4	2.8	3.4
(2*S*)-methylmyristoyl-CoA[d]	2.8	3.2	3.0	2.8
2-meAcAc-CoA[e]	2.9	3.6	2.7	3.0
QM-*S*-IBUCOA[f]	3.9	3.3	3.3	2.8
QM-TS1[f]	3.2	3.4	3.1	2.7
QM-INT[f]	3.6	3.0	3.4	2.6
QM-TS2[f]	3.1	3.0	3.2	3.5
QM-*R*-IBUCOA[f]	3.2	2.9	3.2	3.8
QM-MD-*R*-IBUCOA	3.5	2.9	3.7	4.0

[a]2GD2, active site A. [b]2GCE, active site C. [c]2GCI, active site B. [d]2GD0, active site B. [e]2YIM, active site A. [f]The geometries have been taken from the TS optimization calculations (Figure 8).

dx.doi.org/10.1021/jp210185m | *J. Phys. Chem. B* 2012, 116, 3619–3629

Asp156 is deprotonated, whereas the His126-Glu241* pair is protonated. In order to catalyze the next (*S*)- to (*R*)-conversion, proton exchange of this proton from the His126−Glu241* pair back to Asp156 is required. In the unliganded structure, the active site is well hydrated, and both His126 and Asp156 are exposed to bulk solvent, facilitating the rapid proton exchange between these residues either directly via structured waters or via bulk solvent, and thereby restoring the active site competent for catalyzing the next (*S*)- to (*R*)- conversion, once the product has dissociated from the active site.

Recently, enzyme NMR mechanistic studies have also been reported on human AMACR,[23] using 2-methyldecanoyl-CoA as the substrate. NMR measurements in D_2O show that the levels of residual substrate deuteration by AMACR are higher than those observed for some classical two-base racemases, such as mandelate racemase.[5,69] The substrate of the latter racemase is a small molecule, mandelate, whereas in MCR the substrate is anchored to the enzyme via the bulky CoA moiety. From the structure of the competent MCR-substrate complex, it appears that in this complex the catalytic acid/base residues, His126 and Asp156 are buried, and not in rapid proton exchange with bulk solvent. The incorporation of deuterium in substrate can happen if the catalytic end of the substrate does not diffuse away from the active site after the first catalytic cycle, but remains anchored by its CoA moiety to the enzyme and is involved in at least one more catalytic cycle before leaving the active site completely, allowing the catalytic bases to exchange deuterium from the solvent between product release and binding of a new substrate.[20] This would explain the incorporation of deuterium into the substrate. It also is consistent with the notion that in the unliganded active site, the His126 and Asp156 residues are in rapid proton exchange with solvent.

A critical component of the active site is the oxyanion hole, stabilizing the negative charge on the thioester oxygen atom of the reaction intermediate. The importance of oxyanion holes for stabilizing the negative charge on the oxygen of the thioester enolate is well known.[70−72] The NMR studies of the mode of binding of acetoacetyl-CoA to a medium chain acyl-CoA dehydrogenase show that the thioester moiety adopts a planar sp^2 enolate configuration when bound to this active site.[73] Table 3 lists the distances of the possible hydrogen bond donors (HBDs) of this oxyanion hole (OAH). All HBDs are provided by the protein; water molecules are not involved in this geometry. Several important aspects of this OAH can be noted, for example, (i) two of the three possible HBDs are also involved in the catalytic mechanism of proton abstraction/donation (Nδ1 (His126) and Oδ2/Oδ1 (Asp156)); only one HBD (N (Asp127)) is a main chain HBD; and (*ii*) the protonation state of the peptide NH moiety is well-defined, but the protonation states of the Oδ2/Oδ1(Asp156) and Nδ1-(His126) moieties in the experimental structures are not known a priori. The relatively short O1−Oδ1/Oδ2 (Asp156) distances (Table 3) suggest that in each of the experimental structures Oδ1/Oδ2 (Asp156) is predominantly protonated. The relatively long Nδ1 (His126)−O1 distance in each of the experimental structures (Table 3) suggests that Nδ1 (His126) is unprotonated in these structures. Although it is possible that in the experimental structures the protonation states are mixtures of partly protonated/partly unprotonated side chains, the analysis of these structures suggests that each of these active sites are protonated at Oδ1/Oδ2 (Asp156), but not at Nδ1(His126). Therefore, each of these structures images an active site competent for catalyzing the conversion of the (*S*)-substrate into the (*R*)-substrate.

The QM calculations show that in the intermediate enolate structure both Nδ1 (His126) and Oδ1/Oδ2 (Asp156) are hydrogen bonded to the thioester oxyanion (Figure 7 and Table 3). There is good agreement between the experimental and QM-HBD geometry in the active site (Tables 2 and 3), except for the N (Asp127)−O1 hydrogen bond, which is relatively long in the QM-structure. This might reflect the influence of a longer and more hydrophobic tail in the experimental structures (Chart 1). It is also interesting to note that the N (Asp127) peptide unit is part of an extended hydrogen bond network via O (His126), being hydrogen bonded to N (Asn129) and N (Tyr130); perhaps a larger QM-model including the atoms of these hydrogen bond partners of O (His126) is important for the optimal description of this geometry. Very short hydrogen bonds[25] are not observed in any of the experimental and calculated structures listed in Tables 2 and 3.

The precise geometry in the OAH of the experimental structure of the enzyme complexed with 2-meAcAc-CoA is highlighted in Figure 9 and Table 4. The optimal geometry of a hydrogen bond between a thioester carbonyl oxygen with its HBD is achieved when the C2−C1−O1−HBD dihedral is 0° or 180° (the *in-plane* geometry), with the C1−O1−HBD angle being 120°, allowing for an optimal interaction of the HBD with the lone electron pair orbitals of the oxygen atom.[37] In the experimental structures of the MCR-substrate active site, none of the hydrogen bond partners is optimally oriented for hydrogen bonding with the thioester carbonyl (Table 4), as most of the dihedral values are close to 90°. Interestingly, this preference of hydrogen bonding geometry of the O1-atom of the bound enolate intermediate is different from the bound thioester substrate oxygen. In this intermediate of the reaction, the thioester oxygen is more negatively charged, and the preferred hydrogen bond directionality is much less prominent.[37] Therefore, the MCR active site geometry is more complementary to the enolate intermediate than to the substrate. This observation agrees with studies of other OAH-dependent reaction mechanisms that have an enolate intermediate.[70,74,75] It also agrees with the notion that the geometries of enzyme active sites are much more complementary

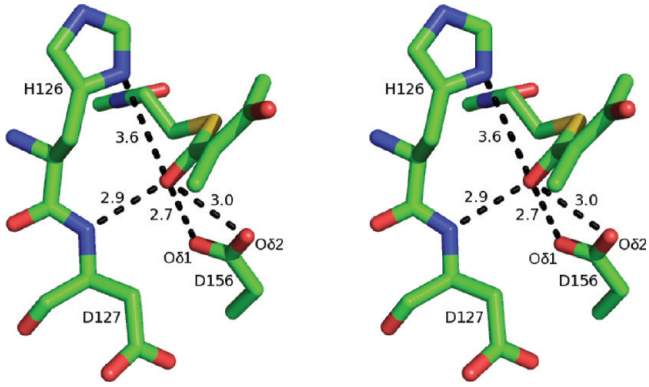

Figure 9. The HBD geometry in the OAH of the crystal structure of the 2-meAcAc-CoA complex. The dotted lines mark the hydrogen bonds between the thioester oxygen and the active site protein atoms.

dx.doi.org/10.1021/jp210185m | *J. Phys. Chem. B* 2012, 116, 3619−3629

Table 4. The Geometry of the OAH

	C2−C1−O1−HBD dihedral (deg)			C1−O1−HBD angle (deg)			O1-HBD distance (Å)		
HBD	reac[a]	int[b]	prod[c]	reac[a]	int[b]	prod[c]	reac[a]	int[b]	prod[c]
Nδ1(His126)	80.0	85.2	98.8	68.9	65.8	72.6	3.3	3.6	3.3
Oδ1(Asp156)	−132.0	−110.9	−91.6	102.5	113.6	99.5	3.1	2.7	2.9
Oδ2(Asp156)	−93.6	−80.2	−64.7	83.3	80.1	67.8	2.9	3.0	3.3
N(Asp127)	86.3	41.8	19.1	164.7	154.0	146.0	3.0	2.9	2.9

[a]MCR complex with (2*S*)-ibuprofenoyl-CoA (2GCE). [b]MCR complex with 2meAcAc-CoA (2YIM). [c]MCR complex with (2*R*)-ibuprofenoyl-CoA (2GCE).

to the transition state as compared to the substrate, favoring catalysis.[76,77]

4. CONCLUDING REMARKS

The high-resolution crystal structure of the 2-meAcAc-CoA MCR complex images the active site interactions of a thioester enolate. This molecule is a reaction intermediate in the catalytic interconversion of the (*S*)-substrate into the (*R*)-product. Both the experimental data as well as the QM/MM calculations show the rigidity of the active site. The calculations support the presence of a planar enolate intermediate and show that both catalytic residues, Asp156 and His126, are also HBDs of the OAH. The *off-plane* geometry of the latter HBDs in the substrate and product thioester complexes shows that better hydrogen bonding to the thioester oxygen is provided in the complex of the enzyme and its enolate reaction intermediate.

■ ASSOCIATED CONTENT

Supporting Information

Complete ref 60. This material is available free of charge via the Internet at http://pubs.acs.org/.

■ AUTHOR INFORMATION

Corresponding Author

*E-mail: rik.wierenga@oulu.fi. Phone: +358 (0)8 553 1199. Fax: +358 (0)8 553 1141.

Present Address

[‖]Department of Biosciences and Bioengineering, Indian Institute of Technology Bombay, Powai, Mumbai-400076, India.

Notes

The authors declare no competing financial interest.

■ ACKNOWLEDGMENTS

We thank Paivi Pirilla for providing us with the 2-methylacetoacetyl-CoA. We thank the beamline scientists of ID14-2 for excellent support. We thank CSC (Center of Scientific Computing) in Espoo (Finland) for providing computing power. This work was supported by grants from the Academy of Finland and the Sigrid Juselius Foundation.

■ REFERENCES

(1) Savolainen, K.; Bhaumik, P.; Schmitz, W.; Kotti, T. J.; Conzelmann, E.; Wierenga, R. K; Hiltunen, J. K. *J. Biol. Chem.* **2005**, *280*, 12611−12620.

(2) Lloyd, M. D.; Darley, D. J.; Wierzbicki, A. S.; Threadgill, M. D. *FEBS J.* **2008**, *275*, 1089−1102.

(3) Tanner, M. E.; Kenyon, G. L. In *Comprehensive Biological Catalysis: A Mechanistic Reference*; Sinnott, M., Ed.; Academic Press: San Diego, 1998; Vol. 2, pp 7−42.

(4) Tanner, M. E. *Acc. Chem. Res.* **2002**, *35*, 237−246.

(5) Mitra, B.; Kallarakal, A. T.; Kozarich, J. W.; Gerlt, J. A.; Clifton, J. G.; Petsko, G. A.; Kenyon, G. L. *Biochemistry* **1995**, *34*, 2777−2787.

(6) St. Maurice, M.; Bearne, S. L. *Biochemistry* **2002**, *41*, 4048−4058.

(7) Bourque, J. R.; Bearne, S. L. *Biochemistry* **2008**, *47*, 566−578.

(8) Cuebas, D. A.; Phillips, C.; Schmitz, W.; Conzelmann, E.; Novikov, D. K. *Biochem. J.* **2002**, *363*, 801−807.

(9) Bhaumik, P.; Schmitz, W.; Hassinen, A.; Hiltunen, J. K.; Conzelmann, E.; Wierenga, R. K. *J. Mol. Biol.* **2007**, *367*, 1145−1161.

(10) Schmitz, W.; Helander, H. M.; Hiltunen, J. K.; Conzelmann, E. *Biochem. J.* **1997**, *326*, 883−889.

(11) van Veldhoven, P. P.; Croes, K.; Asselberghs, S.; Herdewijn, P.; Mannaerts, G. P. *FEBS Lett.* **1996**, *388*, 80−84.

(12) Shefer, S.; Cheng, F. W.; Batta, A. K.; Dayal, B.; Tint, G. S.; Salen, G.; Mosbach, E. H. *J. Biol. Chem.* **1978**, *253*, 6386−6392.

(13) Ferdinandusse, S.; Denis, S.; Clayton, P. T.; Graham, A.; Rees, J. E.; Allen, J. T.; McLean, B. N.; Brown, A. Y.; Vreken, P.; Waterham, H. R.; Wanders, R. J. *Nat. Genet.* **2000**, *24*, 188−191.

(14) Savolainen, K.; Kotti, T. J.; Schmitz, W.; Savolainen, T. I.; Sormunen, R. T.; Ilves, M.; Vainio, S. J.; Conzelmann, E.; Hiltunen, J. K. *Hum. Mol. Genet.* **2004**, *13*, 955−965.

(15) Schmitz, W.; Fingerhut, R.; Conzelmann, E. *Eur. J. Biochem.* **1994**, *222*, 313−323.

(16) Schmitz, W.; Albers, C.; Fingerhut, R.; Conzelmann, E. *Eur. J. Biochem.* **1995**, *231*, 815−822.

(17) Arenskötter, Q.; Heller, J.; Dietz, D.; Arenskötter, M.; Steinbüchel, A. *Appl. Environ. Microbiol.* **2008**, *74*, 7085−7089.

(18) Lee, K. S.; Park, S. M.; Rhee, K. H.; Bang, W. G.; Hwang, K. Y.; Chi, Y. M. *Proteins* **2006**, *64*, 817−822.

(19) Ouazia, D.; Bearne, S. L. *Anal. Biochem.* **2010**, *398*, 45−51.

(20) Kumaresan, K.; Kakkar, N.; Verma, A.; Mandal, A. K.; Singh, S. K.; Joshi, K. *Diagn. Pathol.* **2010**, *5*, 83.

(21) Ouyang, B.; Leung, Y. K.; Wang, V.; Chung, E.; Levin, L.; Bracken, B.; Cheng, L.; Ho, S. M. *Urology* **2011**, *77*, 249.e1−249.e7.

(22) Carnell, A. J.; Hale, I.; Denis, S.; Wanders, R. J.; Isaacs, W. B.; Wilson, B. A.; Ferdinandusse, S. *J. Med. Chem.* **2007**, *50*, 2700−2707.

(23) Darley, D. J.; Butler, D. S.; Prideaux, S. J.; Thornton, T. W.; Wilson, A. D.; Woodman, T. J.; Threadgill, M. D.; Lloyd, M. D. *Org. Biomol. Chem.* **2009**, *7*, 543−552.

(24) Sattar, F. A.; Darley, D. J.; Politano, F.; Woodman, T. J.; Threadgill, M. D.; Lloyd, M. D. *Chem. Commun.* **2010**, *46*, 3348−3350.

(25) Frey, P. A.; Hegeman, A. D. *Enzymatic Reaction Mechanisms*; Oxford University Press: New York, 2007.

(26) St. Maurice, M.; Bearne, S. L. *Biochemistry* **2000**, *39*, 13324−13335.

(27) van der Kamp, M. W.; Perruccio, F.; Mulholland, A. J. *J. Mol. Graphics Modell.* **2007**, *26*, 676−690.

(28) Bell, A. F.; Wu, J.; Feng, Y.; Tonge, P. J. *Biochemistry* **2001**, *40*, 1725−1733.

(29) Merilainen, G.; Poikela, V.; Kursula, P.; Wierenga, R. K. *Biochemistry* **2009**, *48*, 11011−11025.

(30) Hedstrom, L. *Chem. Rev.* **2002**, *102*, 4501−4523.

(31) Harel, M.; Quinn, D. M.; Nair, H. K.; Sisman, I.; Sussman, J. L. *J. Am. Chem. Soc.* **1996**, *118*, 2340−2346.

(32) Pihko, P.; Rapakko, S.; Wierenga, R. K. In *Hydrogen Bonding in Organic Synthesis*; Pihko, P., Ed.; Wiley-VCH Verlag GmbH & Co. KGaA: Weinheim, Germany; 2009; pp 43−71.

(33) Hamed, R.; Batchelar, E.; Clifton, I.; Schofield, C. *Cell. Mol. Life Sci.* **2008**, *65*, 2507−2527.
(34) Venkatesan, R.; Kapetaniou, E. G.; Wierenga, R. K. *Cell. Mol. Life Sci.* **2010**, *67*, 3961−3982.
(35) Houk, R. J.; Monzingo, A.; Anslyn, E. V. *Acc. Chem. Res.* **2008**, *41*, 401−410.
(36) Kraut, D. A.; Sigala, P. A.; Pybus, B.; Liu, C. W.; Ringe, D.; Petsko, G. A; Herschlag, D. *PLoS Biol.* **2006**, *4*, e99.
(37) Papai, I.; Hamza, A.; Pihko, P. M.; Wierenga, R. K. *Chem.—Eur. J.* **2011**, *17*, 2859−2866.
(38) Wilmouth, R. C.; Edman, K.; Neutze, R.; Wright, P. A.; Clifton, I. J.; Schneider, T. R.; Schofield, C. J.; Hajdu, J. *Nat. Struct .Biol.* **2001**, *8*, 689−694.
(39) Liu, B.; Schofield, C. J.; Wilmouth, R. C. *J. Biol. Chem.* **2006**, *281*, 24024−24035.
(40) Haapalainen, A. M.; Meriläinen, G.; Pirilä, P. L.; Kondo, N.; Fukao, T.; Wierenga, R. K. *Biochemistry* **2007**, *46*, 4305−4321.
(41) Kabsch, W. *J. Appl. Crystallogr.* **1993**, *26*, 795−800.
(42) Kabsch, W. *Acta Crystallogr.* **2010**, *D66*, 133−144.
(43) Collaborative Computational Project, Number 4 (CCP4). *Acta Crystallogr.* **1994**, *D50*, 760−763.
(44) Vagin, A.; Teplyakov, A. *J. Appl. Crystallogr.* **1997**, *30*, 1022−1025.
(45) Murshudov, G. N.; Vagin, A. A.; Dodson, E. J. *Acta Crystallogr.* **1997**, *D53*, 240−255.
(46) Emsley, P.; Cowtan, K. *Acta Crystallogr.* **2004**, *D60*, 2126−2132.
(47) DeLano, W. L. *The PyMOL Molecular Graphics System*, 2002 (http://www.pymol.org).
(48) Sali, A.; Blundell, T. L. *J. Mol. Biol.* **1993**, *234*, 779−815.
(49) Berendsen, H. J. C.; Postma, J. P. M.; Van Gunsteren, W. F.; Hermans, J. In *Intermolecular Forces*; Pullman, B., Ed.; Reidel: Dordrecht, The Netherlands, 1981; pp 331−342.
(50) Berendsen, H. J. C.; Postma, J. P. M; DiNola, A.; Van Gunsteren, W. F.; Haak, J. R. *J. Chem. Phys.* **1984**, *181*, 3684−3690.
(51) Darden, T.; York, D.; Pedersen, L. *J. Chem. Phys.* **1993**, *98*, 10089−10092.
(52) Hess, B.; Bekker, H.; Berendsen, H. J. C.; Fraaije, J. G. E. M. *J. Comput. Chem.* **1997**, *18*, 1463−1473.
(53) Van Der Spoel, D.; Lindahl, E.; Hess, B.; Groenhof, G.; Mark, A. E.; Berendsen, H. J. C. *J. Comput. Chem.* **2005**, *26*, 1701−1718.
(54) Hess, B.; Kutzner, C.; Van Der Spoel, D.; Lindahl, E. *Mol. Simul.* **2008**, *4*, 435−447.
(55) Sorin, E. J.; Pande, V. S. *Biophys. J.* **2005**, *88*, 2472−2493.
(56) Cummins, P. L.; Ramnarayan, K.; Singh, U. C.; Gready, J. E. *J. Am. Chem. Soc.* **1991**, *113*, 8247−8256.
(57) Pearlman, D. A.; Case, D. A.; Caldwell, J. W.; Ross, W. R.; Cheatham, I. T. E.; De-Bolt, S.; Ferguson, D.; Seibel, G.; Kollman, P. *Comput. Phys. Commun.* **1995**, *91*, 1−41.
(58) Kwiecien, R. A.; Khavrutskii, I. V.; Musaev, D. G.; Morokuma, K.; Banerjee, R.; Paneth, P. *J. Am. Chem. Soc.* **2006**, *128*, 1287−1292.
(59) Svensson, M.; Humbel, S.; Froese, R. D. J.; Matsubara, T.; Sieber, S.; Morokuma, K. *J. Phys. Chem.* **1996**, *100*, 19357−19363.
(60) Frisch, M. J.; Trucks, G. W.; Schlegel, H. B.; Scuseria, G. E.; Robb, M. A.; Cheeseman, J. R.; Scalmani, G.; Barone, V.; Mennucci, B.; Petersson, G. A., et al. *Gaussian 09, Revision A.1*; Gaussian, Inc.: Wallingford, CT, 2009.
(61) Wang, J.; P., C.; Kollman, P. A. *J. Comput. Chem.* **2000**, *21*, 1049−1074.
(62) *MatLab*, version, 7.7; The Math Works, Inc: Natick, MA, 2008.
(63) Breneman, C. M.; Wiberg, K. B. *J. Comput. Chem.* **1990**, *11*, 361−373.
(64) Heinson, C. D.; Williams, J. M.; Tinnerman, W. N.; Malloy, T. B. *J. Chem. Educ.* **2005**, *82*, 787−789.
(65) Auer, H. E.; Frerman, F. E. *J. Biol. Chem.* **1980**, *255*, 8157−8163.
(66) Richard, J. P.; Amyes, T. L. *Curr. Opin. Chem. Biol.* **2001**, *5*, 626−633.
(67) van der Kamp, M. W.; Perruccio, F.; Mulholland, A. J. *Proteins* **2007**, *69*, 521−535.
(68) Yang, W.; Drueckhammer, D. G. *J. Phys. Chem. B* **2003**, *107*, 5986−5994.
(69) Bearne, S. L.; Wolfenden, R. *Biochemistry* **1997**, *36*, 1646−1656.
(70) Simón, L.; Goodman, J. M. *J. Org. Chem.* **2010**, *75*, 1831−1840.
(71) Hamed, R. B.; Batchelar, E. T.; Clifton, I. J.; Schofield, C. J. *Cell. Mol. Life Sci.* **2008**, *65*, 2507−2527.
(72) Zhang, H.; Machutta, C. A.; Tonge, P. J. In *Comprehensive Natural Products Chemistry II: Chemistry and Biology*; Mander, L., Lui, H.-W., Eds.; Elsevier: Oxford, 2010; Vol. 8, pp 231−275.
(73) Nishina, Y.; Sato, K.; Tamaoki, H.; Tanaka, T.; Setoyama, C.; Miura, R.; Shiga, K. *J. Biochem.* **2003**, *134*, 835−842.
(74) Xu, D.; Wei, Y.; Wu, J.; Dunaway-Mariano, D.; Guo, H.; Cui, Q.; Gao, J. *J. Am. Chem. Soc.* **2004**, *126*, 13649−13658.
(75) Luo, L.; Taylor, K. L.; Xiang, H.; Wei, Y.; Zhang, W.; Dunaway-Mariano, D. *Biochemistry* **2001**, *40*, 15684−15692.
(76) Schramm, V. L. *J. Biol. Chem.* **2007**, *282*, 28297−28300.
(77) Wolfenden, R. *Nature* **1969**, *223*, 704−705.